Kinoshita, M., Tobin, H., Ashi, J., Kimura, G., Lallemant, S., Screaton, E.J., Curewitz, D., Masago, H., Moe, K.T., and the Expedition 314/315/316 Scientists
Proceedings of the Integrated Ocean Drilling Program, Volume 314/315/316

Data report: frictional strength of mudstone samples from the Nankai Trough frontal thrust region, IODP Sites C0006 and C0007[1]

Matt J. Ikari[2] and Andre Hüpers[2]

Chapter contents

[1]Ikari, M.J., and Hüpers, A., 2019. Data report: frictional strength of mudstone samples from the Nankai Trough frontal thrust region, IODP Sites C0006 and C0007. *In* Kinoshita, M., Tobin, H., Ashi, J., Kimura, G., Lallemant, S., Screaton, E.J., Curewitz, D., Masago, H., Moe, K.T., and the Expedition 314/315/316 Scientists, *Proceedings of the Integrated Ocean Drilling Program,* 314/315/316: Washington, DC (Integrated Ocean Drilling Program Management International, Inc.). doi:10.2204/iodp.proc.314315316.224.2019
[2]MARUM Center for Marine Environmental Sciences and Faculty of Geosciences, University of Bremen, Germany. Correspondence author: mikari@marum.de

Abstract

We conducted shearing tests on samples from the frontal thrust region of the Nankai Trough offshore Kii Peninsula, Japan, recovered from Sites C0006 and C0007 during Integrated Ocean Drilling Program (IODP) Expedition 316. The samples are all silty clay recovered from 192–561 meters below seafloor and corresponding to Units II and III. Samples were sheared in a double-direct shear configuration in a true-triaxial pressure vessel that was confined and under fluid pressure control. We observed that residual shear strength values increase sublinearly over effective normal stresses from 5 to 35 MPa. Residual friction coefficients calculated from the measured shear strength and effective normal stress range from 0.22 to 0.56 and decrease as a function of increasing effective normal stress. For each sample, the data for coefficient of friction as a function of increasing effective normal stress are equally well fit by power law and logarithmic relations. Sample 316-C0006F-19R-1 is noticeably weaker than the other samples, which can be attributed to its high clay mineral content of 67 wt%.

Introduction

Frictional strength is an important basic geotechnical parameter for sediment deformation because the strength controls the structure and faulting processes in convergent margins. Here, we measured the frictional strength on five core samples at a range of effective normal stresses in order to establish basic strength measurements for the frontal thrust region of the Nankai Trough. Such strength measurements may be used for studies of shallow fault slip (Kopf and Brown, 2003; Ikari and Saffer, 2011) or studies of accretionary wedge geometry (Kimura et al., 2007; Ikari et al., 2013). The samples we tested were recovered during Integrated Ocean Drilling Program (IODP) Expedition 316, part of the Nankai Trough Seismogenic Zone Experiment (NanTroSEIZE). During NanTroSEIZE, several sites were drilled and cored along a transect offshore Kii peninsula, Japan (Figure F1). We focus on two sites in the frontal thrust region, Sites C0006 and C0007.

Site and sample description

Sites C0006 and C0007 are located less than ~2 km landward of the deformation front in the Nankai Trough. The region is a zone

doi:10.2204/iodp.proc.314315316.224.2019

of diffuse faulting that may act as the plate boundary (Screaton et al., 2009). The main frontal thrust was not penetrated at Site C0006 but was penetrated at Site C0007 slightly trenchward (Figure F2). We tested four samples from Site C0006 (see the "Expedition 316 Site C0006" chapter [Expedition 316 Scientists, 2009a]) and one sample from Site C0007 (see the "Expedition 316 Site C0007" chapter [Expedition 316 Scientists, 2009b]), which were recovered from 192–562 meters below seafloor (mbsf) (Table T1). All samples are described lithologically as silty clay, of which the uppermost four samples belong to Unit II, representing accreted trench wedge sediments, whereas the deepest sample, 316-C0006F-19R-1 from Unit III, has been classified as accreted Shikoku Basin sediment. The samples are not from any major fault or zone of concentrated deformation and therefore represent wall rock mudstone for the frontal thrust region. Bulk composition of the samples was quantified by shipboard X-ray diffraction (see the "Expedition 316 Site C0006" and "Expedition 316 Site C0007" chapters [Expedition 316 Scientists, 2009a, 2009b]). Total clay mineral content for our tested samples ranges from 41 to 67 wt% with the remainder being quartz and plagioclase except for 5 wt% calcite observed in Sample 316-C0006F-7R-1 (Table T1).

Experimental methods

We conducted laboratory shearing experiments under true-triaxial stress conditions and controlled pore pressure, using a biaxial testing apparatus with servo-hydraulic control (Figure F3). Samples were constructed as two layers with an area of 5.4 cm × 5.7 cm and initial thicknesses ranging from ~2 to 6 mm under an initial normal stress of 5 MPa. Most of the samples were built remolded, meaning core material was lightly cold-pressed into the sample assembly. One sample, 316-C0006E-40X-8, was tested as two intact wafers trimmed perpendicular to the core axis. The two subsamples were sandwiched in a three-block assembly outfitted with porous metal frits, allowing fluid access, jacketed in rubber. The jacketed assembly was placed in the pressure vessel and subjected to confining pressure and then saturated with 3.5 wt% NaCl brine as pore fluid. The effective normal stress includes the combined effects of externally applied normal load, confining pressure, and two independent pore pressures. One of the pore pressures was applied to the inner faces of the sample layers and designated as the inlet pressure; the other pore pressure accesses the outer faces of the samples and was designated as the outlet pressure (Figure F3). The confining pressure was held constant at 6 MPa and the inlet pore pressure was held constant at 5 MPa. The outlet pressure was set to a no-flow (undrained) condition to monitor pore pressure in the layer during shearing, following Ikari and Saffer (2011). Pore pressure fluctuations recorded by the outlet pressure are accounted for in calculating the effective normal stress; these fluctuations are small and have little effect on the experiment (Figure F4). With the confining and pore pressures held constant, the effective normal stress was raised from 5 to 15, 25, and 35 MPa by increasing the externally applied normal load (Figure F4).

In each experiment, we sheared our samples at a constant driving rate boundary condition of 11 µm/s, as measured at the load cell on the vertical piston (i.e., load point velocity). The shear stress τ is measured continuously, from which we calculate a coefficient of sliding friction μ (Handin, 1969):

$$\tau = \mu\sigma_n',$$

where $\mu\sigma_n'$ is the effective normal stress. Note that in calculating a sliding coefficient of friction we assume that the shear strength results entirely from frictional strength and there is no cohesive strength component. This facilitates comparison with previous studies, but we acknowledge that the cohesion in sheared materials may be significant (Ikari and Kopf, 2011).

Peak shear strength was measured only at the lowest effective normal stress (5 MPa) because the higher effective normal stresses tested in this study are much higher than the in situ effective stresses experienced by the samples. Residual shear strength was measured at every effective normal stress. In some cases, the sample reached a steady state; however, in many cases a slight slip strengthening or weakening trend was superimposed on the data (Table T2). In the case of slip weakening, we measured the maximum strength. In slip strengthening cases, we calculated a strengthening rate as $d\tau/dx$, where x is displacement, and picked the strength value where $d\tau/dx$ became constant (see Ikari et al., 2011).

Results

Residual shear strength increases from ~2.5 MPa at σ_n' = 5 MPa to 12–14 MPa at σ_n' = 35 MPa for most samples (Figure F5; Table T2). Sample 316-C0006F-19R-1 is noticeably weaker than the other samples and increases from 1.3 to 8.6 MPa residual shear strength. Sample 19R-1 is also the only sample to exhibit a significant peak shear strength at σ_n' = 5 MPa, whereas for the other samples the peak strength is

not significantly higher than the residual shear strength (Table T2).

For all samples, residual shear strength increases as a function of effective normal stress, similar to Coulomb-Mohr behavior. However, our samples did not strictly exhibit Coulomb-Mohr behavior but rather sublinear shear strength as a function of effective normal stress. This can be seen in the values of residual coefficient of friction, which decrease as a function of effective normal stress (Figure F6; Table T2). For most samples, residual μ ranges from 0.46 to 0.56 at σ_n' = 5 MPa and decreases to 0.34–0.40 at σ_n' = 35 MPa. The residual μ of the weaker Sample 316-C0006F-19R-1 ranges from 0.22 to 0.27.

A feature of the residual coefficient of friction data is that they decrease nonlinearly with increasing effective normal stress. We fit the data for each sample with both power law and logarithmic functions:

$$\mu = A\sigma_n'^{\omega} \text{ and}$$

$$\mu = B\log_{10}(\sigma_n') + C,$$

where the parameters A, ω, B, and C are empirically determined from the regression. We observe that both power law and logarithmic provided excellent fits to the data for the four stronger samples, with the coefficient of determination R^2 values of at least 0.978 (Figure F7; Table T3). The power law and logarithmic functions provide nearly identical fits to the data.

In contrast to the four stronger samples, the weaker Sample 316-C0006F-19R-1 exhibits a low R^2 value for both the power law and logarithmic fits. It is possible that the reason for this is that the coefficient of friction may show a more significant increase at lower effective normal stresses than the other samples. In general, the unique behavior of this sample can be attributed to its clay mineral content, which is the highest of the five samples at 67 wt% (Figure F8; Table T1). For our data set, we observed a general trend of decreasing coefficient of friction with increasing clay content (Figure F8) with the low friction of Sample 19R-1 being clearly related to high clay content. We note that because we tested mostly remolded samples, our experiments isolate the effect of mineral assemblage. In nature, microstructural differences due to different depositional settings (i.e., trench wedge [Unit II]) compared to hemipelagic basin [Unit II]) sediments) could also play a role (e.g., Takahashi et al., 2013).

Acknowledgments

We thank Chris Marone for access to the Pennsylvania State University Rock and Sediment Mechanics Laboratory and Kyu Kanagawa for a helpful review. Samples were provided by the Integrated Ocean Drilling Program (IODP) and collected during Expedition 316. Funding was provided by the Deutsche Forschungsgemeinschaft via the MARUM Research Center.

References

Expedition 316 Scientists, 2009. Expedition 316 Site C0006. *In* Kinoshita, M., Tobin, H., Ashi, J., Kimura, G., Lallemant, S., Screaton, E.J., Curewitz, D., Masago, H., Moe, K.T., and the Expedition 314/315/316 Scientists, *Proceedings of the Integrated Ocean Drilling Program,* 314/315/316: Washington, DC (Integrated Ocean Drilling Program Management International, Inc.). **https://doi.org/10.2204/iodp.proc.314315316.134.2009**

Expedition 316 Scientists, 2009. Expedition 316 Site C0007. *In* Kinoshita, M., Tobin, H., Ashi, J., Kimura, G., Lallemant, S., Screaton, E.J., Curewitz, D., Masago, H., Moe, K.T., and the Expedition 314/315/316 Scientists, *Proceedings of the Integrated Ocean Drilling Program,* 314/315/316: Washington, DC (Integrated Ocean Drilling Program Management International, Inc.). **https://doi.org/10.2204/iodp.proc.314315316.135.2009**

Handin, J., 1969. On the Coulomb-Mohr failure criterion. *Journal of Geophysical Research: Solid Earth,* 74(22):5343–5348. **https://doi.org/10.1029/JB074i022p05343**

Ikari, M.J., Hüpers, A., and Kopf, A.J., 2013. Shear strength of sediments approaching subduction in the Nankai, Trough, Japan as constraints on forearc mechanics. *Geochemistry, Geophysics, Geosystems,* 14(8):2716–2730. **https://doi.org/10.1002/ggge.20156**

Ikari, M.J., and Kopf, A.J., 2011. Cohesive strength of clay-rich sediment. *Geophysical Research Letters,* 38(16):L16309. **https://doi.org/10.1029/2011GL047918**

Ikari, M.J., Niemeijer, A.R., and Marone, C., 2011. The role of fault zone fabric and lithification state on frictional strength, constitutive behavior, and deformation microstructure. *Journal of Geophysical Research: Solid Earth,* 116(B8):B08404. **https://doi.org/10.1029/2011JB008264**

Ikari, M.J., and Saffer, D.M., 2011. Comparison of frictional strength and velocity dependence between fault zones in the Nankai accretionary complex. *Geochemistry Geophysics Geosystems,* 12(4):Q0AD11. **https://doi.org/10.1029/2010GC003442**

Kimura, G., Kitamura, Y., Hashimoto, Y., Yamaguchi, A., Shibata, T., Ujiie, K., and Okamoto, S., 2007. Transition of accretionary wedge structures around the up-dip

limit of the seismogenic subduction zone. *Earth and Planetary Science Letters,* 225(3–4):471–484. https://doi.org/10.1016/j.epsl.2007.01.005

Kimura, G., Screaton, E.J., Curewitz, D., and the Expedition 316 Scientists, 2008. *Expedition 316 Preliminary Report: NanTroSEIZE Stage 1A: NanTroSEIZE Shallow Megasplay and Frontal Thrusts*. Integrated Ocean Drilling Program. https://doi.org/10.2204/iodp.pr.316.2008

Kopf, A., and Brown, K.M., 2003. Friction experiments on saturated sediments and their implications for the stress state of the Nankai and Barbados subduction thrusts. *Marine Geology,* 202(3–4):193–210. https://dx.doi.org/10.1016/S0025-3227(03)00286-X

Samuelson, J., Elsworth, D., and Marone, C., 2009. Shear-induced dilatancy of fluid-saturated faults: experiment and theory. *Journal of Geophysical Research: Solid Earth,* 114(B12):B12404. https://doi.org/10.1029/2008JB006273

Screaton, E., Kimura, G., Curewitz, D., Moore, G., Fabbri, O., Fergusson, C., Girault, F., et al., 2009. Interactions between deformation and fluids in the frontal thrust region of the NanTroSEIZE transect offshore the Kii Peninsula, Japan: results from IODP Expedition 316 Sites C0006 and C0007. *Geochemistry, Geophysics, Geosystems,* 10(12):Q0AD01. https://doi.org/10.1029/2009GC002713

Takahashi, M., Azuma, S., Uehara, S., Kanagawa, K., and Inoue, A., 2013. Contrasting hydrological and mechanical properties of clayey and silty muds cored from the shallow Nankai Trough accretionary prism. *Tectonophysics,* 600:63–74. https://doi.org/10.1016/j.tecto.2013.01.008

Initial receipt: 18 February 2019
Acceptance: 25 July 2019
Publication: 26 September 2019
MS 314315316-224

Figure F1. Nankai Trough with location of Sites C0006 and C0007 and rupture areas (dashed boxes), and epicenters (stars) of the 1944 Tonankai and 1946 Nankai earthquakes (modified from Kimura et al., 2008). EP = Eurasian plate, PSP = Philippine Sea plate, PP = Pacific plate, NAP = North American plate.

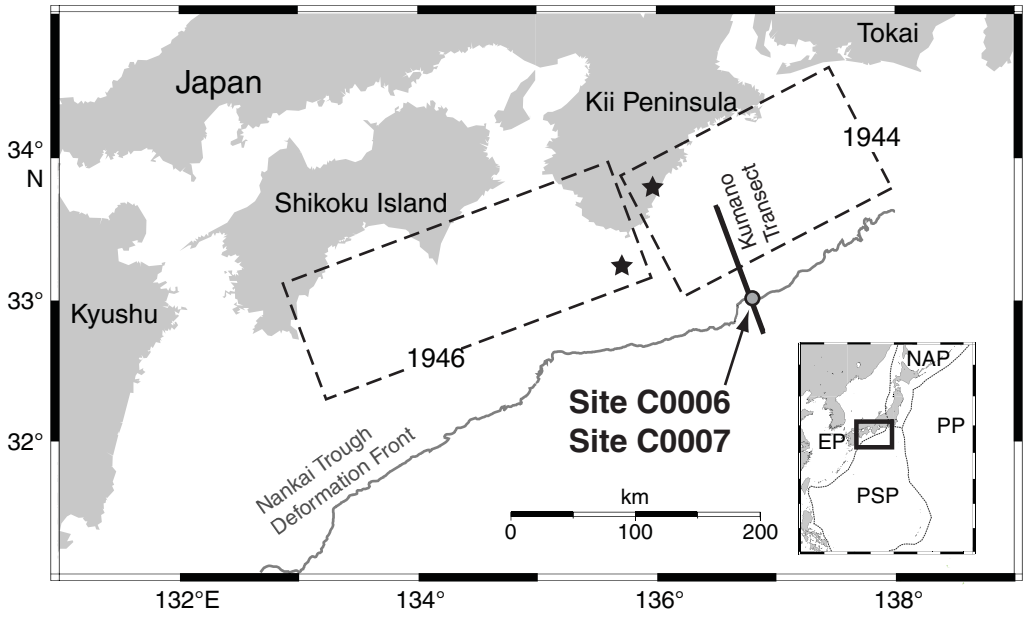

Figure F2. Seismic reflection profile of the frontal thrust region in the accretionary prism along the Kumano transect shown in Figure F1, Sites C0006 and C0007 (modified from Kimura et al., 2008). Blue stars = sample depths. VE = vertical exaggeration.

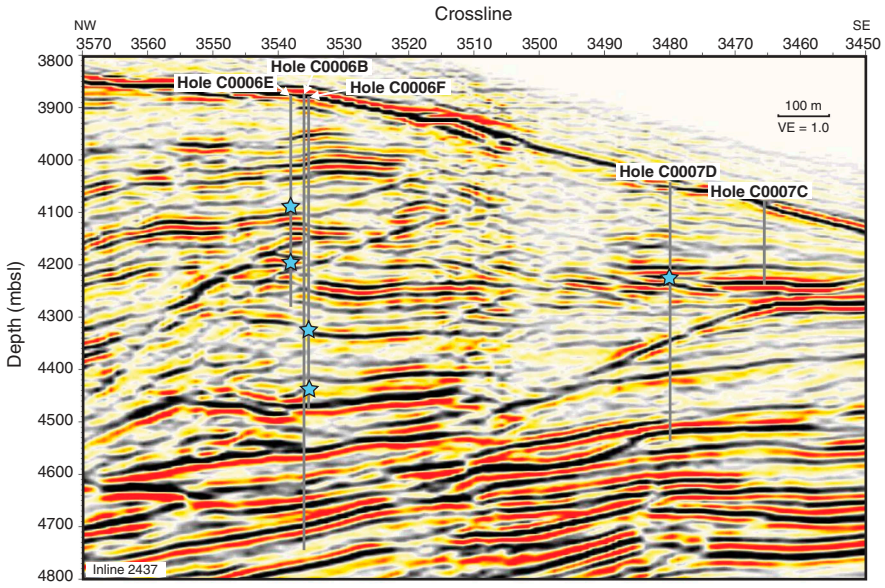

Figure F3. Pressure vessel with sample assembly housed in a biaxial deformation apparatus, Expedition 316 (modified from Samuelson et al., 2009). Half arrows = sense of shear on the sample.

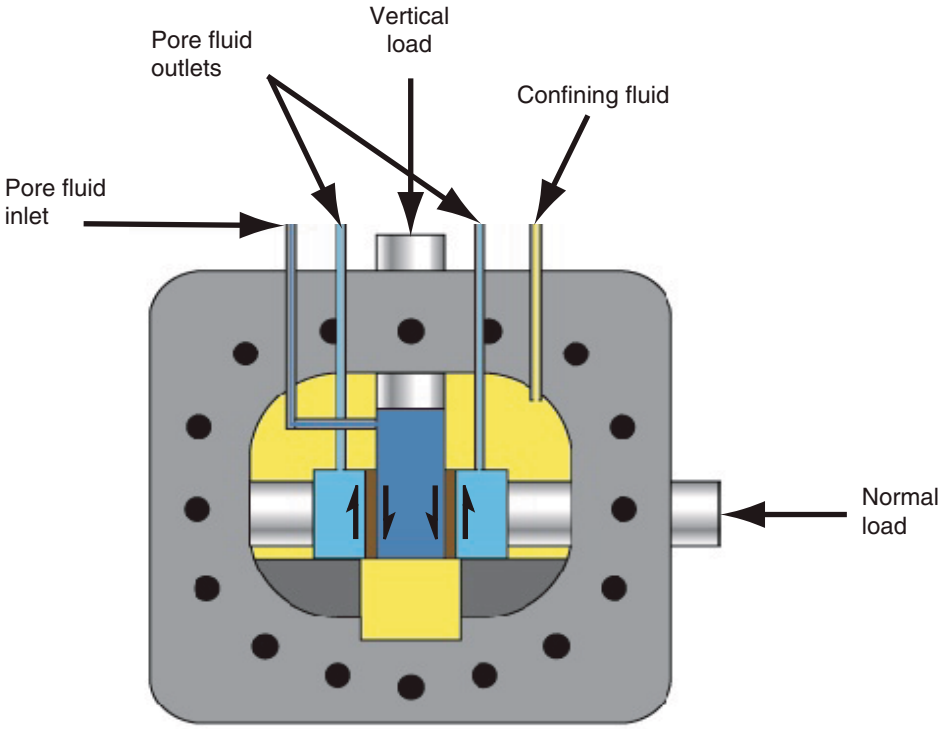

Figure F4. Example of experimental raw data from Sample 316-C0007D-3R-3, showing the measured shear stress and controlled effective normal stress as a function of shear displacement. The effective normal stress includes any potential fluctuations in pore pressure. The nearly constant values show that the effect of pore pressure fluctuations on the shear stress data is negligible.

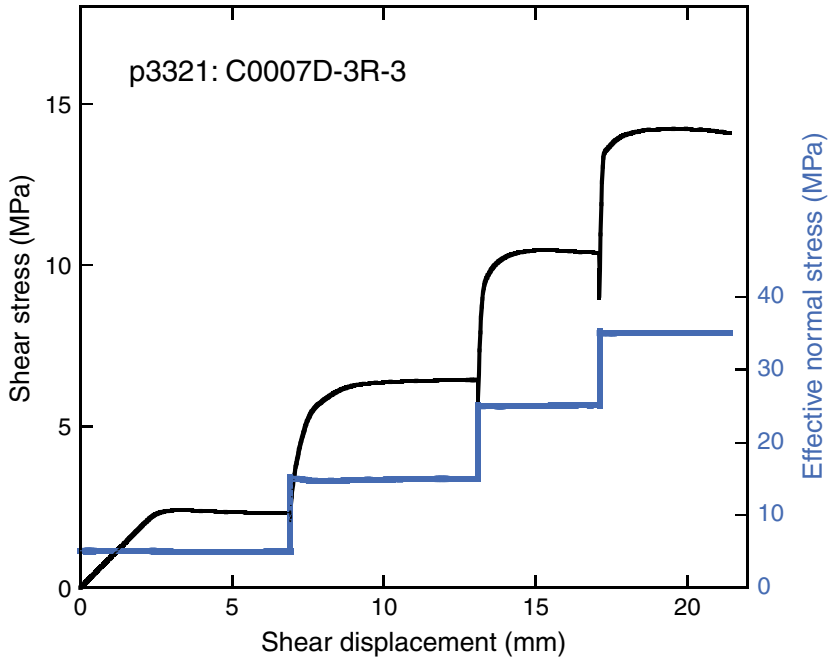

Figure F5. Residual shear strength as a function of effective normal stress for all samples in this study, Sites C0006 and C0007.

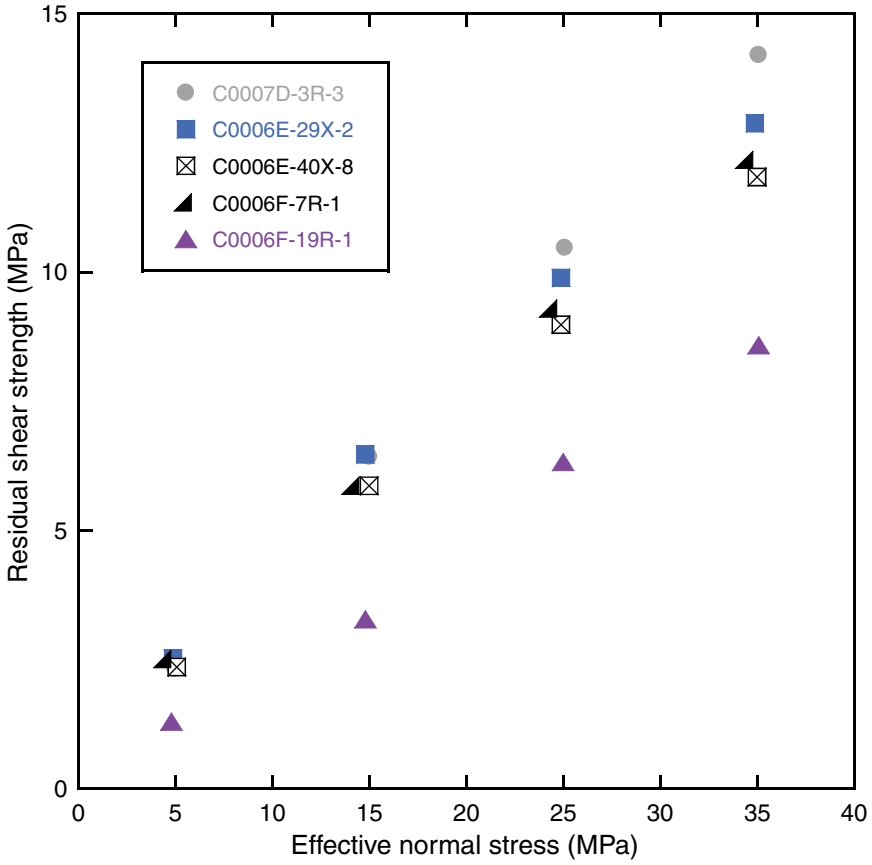

Figure F6. Residual coefficient of friction as a function of effective normal stress for all samples in this study, Sites C0006 and C0007.

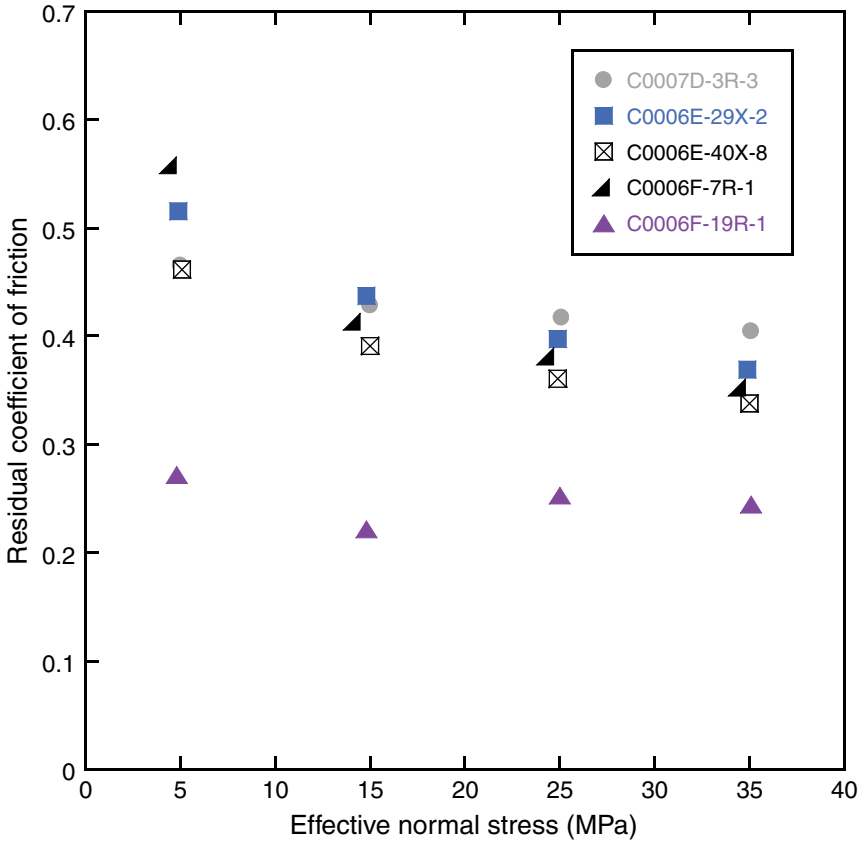

Figure F7. Comparison of (A) Power law and (B) logarithmic fits to the residual coefficient of friction as a function of effective normal stress data shown in Figure F6, Holes C0006 and C0007. Note that the two forms fit the data nearly identically well. See Table T3 for fit parameters.

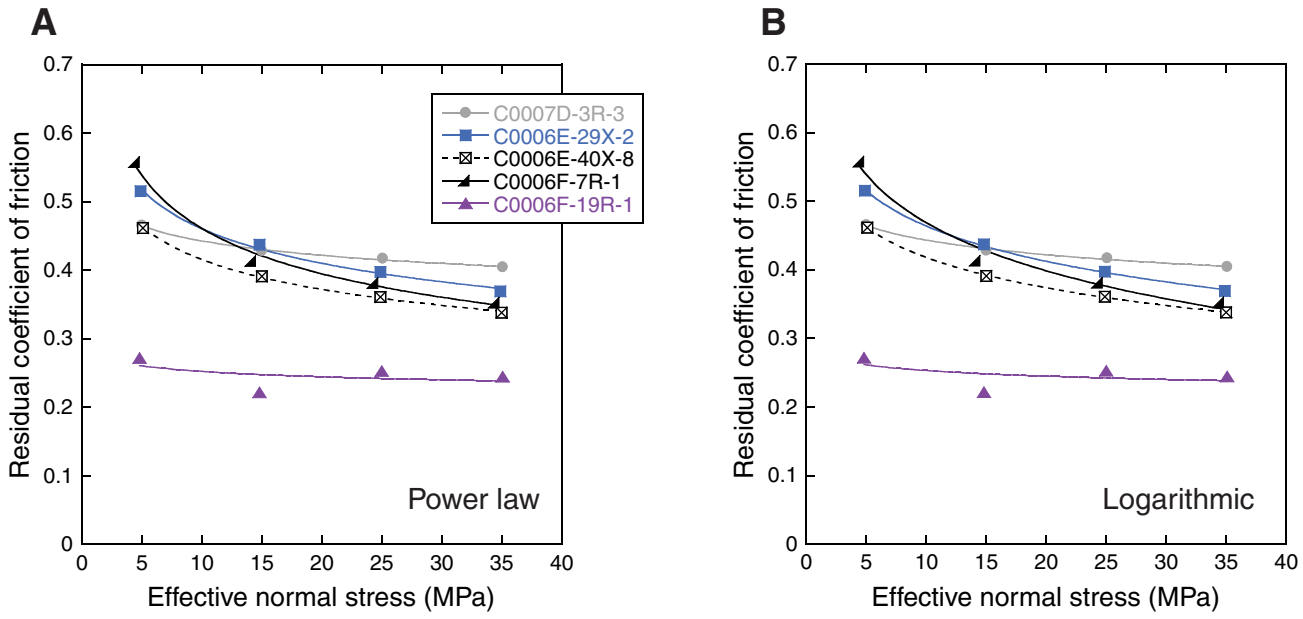

Figure F8. Residual coefficient of friction for all samples in this study as a function of total clay mineral content, Sites C0006 and C0007.

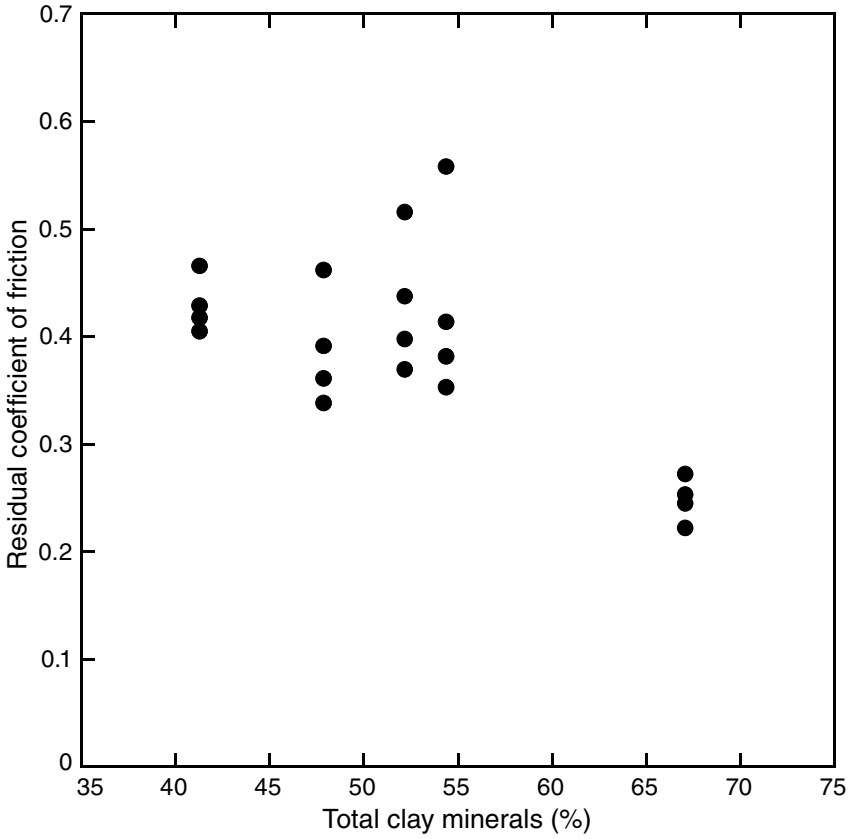

Table T1. Sample details, Site C0006 and C0007.

Experiment	Hole, core, section	Depth (mbsf)	Unit	Lithology	Total clay (%)
	316-				
P3321	C0007D-3R-3	192.35	IIC	Silty clay	41.3
P3325	C0006E-29X-2	213.12	IIC	Silty clay	52.2
P3324	C0006E-40X-8	322.80	IIC	Silty clay	47.9
P3354	C0006F-7R-1	448.10	IID	Silty clay	54.4
P3355	C0006F-19R-1	561.65	III	Silty clay	67.1

Lithology and total clay from the "**Expedition 316 Site C0006**" and "**Expedition 316 Site C0007**" chapters (Expedition 316 Scientists, 2009a, 2009b).

Table T2. Results of shearing experiments, Site C0006 and C0007.

Experiment	Hole, core, section	Depth (mbsf)	Testing condition	σ_n' (MPa)	Peak τ (MPa)	Peak μ	Residual τ (MPa)	Residual μ	Trend description
	316-								
P3321	C0007D-3R-3	192.35	Remolded	5.0	2.41	0.48	2.33	0.47	Steady state
				15.0			6.43	0.43	Steady state
				25.1			10.47	0.42	Slip weakening
				35.1			14.20	0.40	Slip weakening
P3325	C0006E-29X-2	213.12	Remolded	4.9	2.57	0.52	2.52	0.52	Slip weakening
				14.8			6.47	0.44	Steady state
				24.9			9.89	0.40	Steady state
				34.9			12.88	0.37	Slip weakening
P3324	C0006E-40X-8	322.80	Intact	5.1	2.39	0.47	2.35	0.46	Steady state
				15.0			5.87	0.39	Steady state
				24.9			8.98	0.36	Steady state
				35.0			11.83	0.34	Slip weakening
P3354	C0006F-7R-1	448.10	Remolded	4.5	2.51	0.56	2.51	0.56	Slip weakening
				14.2			5.87	0.41	Slip weakening
				24.4			9.30	0.38	Slip weakening
				34.5			12.17	0.35	Slip weakening
P3355	C0006F-19R-1	561.65	Remolded	4.8	1.61	0.33	1.30	0.27	Steady state
				14.8			3.28	0.22	Slip strengthening
				25.0			6.32	0.25	Steady state
				35.1			8.58	0.24	Slip strengthening

Table T3. Curve fits to residual friction data, Site C0006 and C0007.

			Power law			Logarithmic		
Experiment	Hole, core, section	Depth (mbsf)	Coefficient A	Exponent ω	R^2	Coefficient B	Intercept C	R^2
	316-							
P3321	C0007D-3R-3	192.35	0.52	–0.07	0.996	–0.07	0.51	0.995
P3325	C0006E-29X-2	213.12	0.68	–0.17	0.994	–0.17	0.63	0.999
P3324	C0006E-40X-8	322.80	0.60	–0.16	0.999	–0.15	0.57	1.000
P3354	C0006F-7R-1	448.10	0.77	–0.22	0.991	–0.23	0.70	0.978
P3355	C0006F-19R-1	561.65	0.28	–0.05	0.260	–0.03	0.28	0.252